2013

Single Spin Asymmetry AN in Polarized Proton–Proton Elastic Scattering at √s = 200 GeV

L. Adamczyk

G. Agakishiev

M. M. Aggarwal

Z. Ahammed

A. V. Alakhverdyants

See next page for additional authors

Repository Citation

Adamczyk, L.; Agakishiev, G.; Aggarwal, M. M.; Ahammed, Z.; Alakhverdyants, A. V.; Alekseev, I.; Alford, J.; Anson, C. D.; Arkhipkin, D.; Aschenauer, E.; Bültmann, S.; Koralt, I.; and Plyku, D., "Single Spin Asymmetry AN in Polarized Proton–Proton Elastic Scattering at √s = 200 GeV" (2013). *Physics Faculty Publications*. 97.
https://digitalcommons.odu.edu/physics_fac_pubs/97

Original Publication Citation

Adamczyk, L., Agakishiev, G., Aggarwal, M. M., Ahammed, Z., Alakhverdyants, A. V., Alekseev, I., . . . Zyzak, M. (2013). Single spin asymmetry in polarized proton–proton elastic scattering at √s = 200 GeV . *Physics Letters B, 719*(1–3), 62-69. doi:https://doi.org/10.1016/j.physletb.2013.01.014

Authors
L. Adamczyk, G. Agakishiev, M. M. Aggarwal, Z. Ahammed, A. V. Alakhverdyants, I. Alekseev, J. Alford, C. D. Anson, D. Arkhipkin, E. Aschenauer, S. Bültmann, I. Koralt, and D. Plyku

Physics Letters B 719 (2013) 62–69

Contents lists available at SciVerse ScienceDirect

Physics Letters B

www.elsevier.com/locate/physletb

Single spin asymmetry A_N in polarized proton–proton elastic scattering at $\sqrt{s} = 200$ GeV

STAR Collaboration

L. Adamczyk [a], G. Agakishiev [u], M.M. Aggarwal [ah], Z. Ahammed [ba], A.V. Alakhverdyants [u], I. Alekseev [s], J. Alford [v], C.D. Anson [ae], D. Arkhipkin [d], E. Aschenauer [d], G.S. Averichev [u], J. Balewski [z], A. Banerjee [ba], Z. Barnovska [n], D.R. Beavis [d], R. Bellwied [aw], M.J. Betancourt [z], R.R. Betts [j], A. Bhasin [t], A.K. Bhati [ah], H. Bichsel [bc], J. Bielcik [m], J. Bielcikova [n], L.C. Bland [d], I.G. Bordyuzhin [s], W. Borowski [as], J. Bouchet [v], A.V. Brandin [ac], S.G. Brovko [f], E. Bruna [be], S. Bültmann [af], I. Bunzarov [u], T.P. Burton [d], J. Butterworth [an], X.Z. Cai [ar], H. Caines [be], M. Calderón de la Barca Sánchez [f], D. Cebra [f], R. Cendejas [g], M.C. Cervantes [au], P. Chaloupka [m], Z. Chang [au], S. Chattopadhyay [ba], H.F. Chen [ap], J.H. Chen [ar], J.Y. Chen [i], L. Chen [i], J. Cheng [ax], M. Cherney [l], A. Chikanian [be], W. Christie [d], P. Chung [n], J. Chwastowski [k], M.J.M. Codrington [au], R. Corliss [z], J.G. Cramer [bc], H.J. Crawford [e], X. Cui [ap], S. Das [p], A. Davila Leyva [av], L.C. De Silva [aw], R.R. Debbe [d], T.G. Dedovich [u], J. Deng [aq], R. Derradi de Souza [h], S. Dhamija [r], L. Didenko [d], F. Ding [f], A. Dion [d], P. Djawotho [au], X. Dong [y], J.L. Drachenberg [au], J.E. Draper [f], C.M. Du [x], L.E. Dunkelberger [g], J.C. Dunlop [d], L.G. Efimov [u], M. Elnimr [bd], J. Engelage [e], G. Eppley [an], L. Eun [y], O. Evdokimov [j], R. Fatemi [w], S. Fazio [d], J. Fedorisin [u], R.G. Fersch [w], P. Filip [u], E. Finch [be], Y. Fisyak [d], C.A. Gagliardi [au], D.R. Gangadharan [ae], F. Geurts [an], A. Gibson [az], S. Gliske [b], Y.N. Gorbunov [l], O.G. Grebenyuk [y], D. Grosnick [az], S. Gupta [t], W. Guryn [d], B. Haag [f], O. Hajkova [m], A. Hamed [au], L.-X. Han [ar], J.W. Harris [be], J.P. Hays-Wehle [z], S. Heppelmann [ai], A. Hirsch [ak], G.W. Hoffmann [av], D.J. Hofman [j], S. Horvat [be], B. Huang [d], H.Z. Huang [g], P. Huck [i], T.J. Humanic [ae], L. Huo [au], G. Igo [g], W.W. Jacobs [r], C. Jena [ad], E.G. Judd [e], S. Kabana [as], K. Kang [ax], J. Kapitan [n], K. Kauder [j], H.W. Ke [i], D. Keane [v], A. Kechechyan [u], A. Kesich [f], D.P. Kikola [ak], J. Kiryluk [y], I. Kisel [y], A. Kisiel [bb], V. Kizka [u], S.R. Klein [y], D.D. Koetke [az], T. Kollegger [o], J. Konzer [ak], I. Koralt [af], L. Koroleva [s], W. Korsch [w], L. Kotchenda [ac], P. Kravtsov [ac], K. Krueger [b], I. Kulakov [y], L. Kumar [v], M.A.C. Lamont [d], J.M. Landgraf [d], S. LaPointe [bd], J. Lauret [d], A. Lebedev [d], R. Lednicky [u], J.H. Lee [d], W. Leight [z], M.J. LeVine [d], C. Li [ap], L. Li [av], W. Li [ar], X. Li [ak], X. Li [at], Y. Li [ax], Z.M. Li [i], L.M. Lima [ao], M.A. Lisa [ae], F. Liu [i], T. Ljubicic [d], W.J. Llope [an], R.S. Longacre [d], Y. Lu [ap], X. Luo [i], A. Luszczak [k], G.L. Ma [ar], Y.G. Ma [ar], D.M.M.D. Madagodagettige Don [l], D.P. Mahapatra [p], R. Majka [be], O.I. Mall [f], S. Margetis [v], C. Markert [av], H. Masui [y], H.S. Matis [y], D. McDonald [an], T.S. McShane [l], S. Mioduszewski [au], M.K. Mitrovski [d], Y. Mohammed [au], B. Mohanty [ad], M.M. Mondal [au], B. Morozov [s], M.G. Munhoz [ao], M.K. Mustafa [ak], M. Naglis [y], B.K. Nandi [q], Md. Nasim [ba], T.K. Nayak [ba], J.M. Nelson [c], L.V. Nogach [aj], J. Novak [ab], G. Odyniec [y], A. Ogawa [d], K. Oh [al], A. Ohlson [be], V. Okorokov [ac], E.W. Oldag [av], R.A.N. Oliveira [ao], D. Olson [y], P. Ostrowski [bb], M. Pachr [m], B.S. Page [r], S.K. Pal [ba], Y.X. Pan [g], Y. Pandit [v], Y. Panebratsev [u], T. Pawlak [bb], B. Pawlik [ag], H. Pei [j], C. Perkins [e], W. Peryt [bb], P. Pile [d], M. Planinic [bf], J. Pluta [bb], D. Plyku [af], N. Poljak [bf], J. Porter [y], A.M. Poskanzer [y], C.B. Powell [y], C. Pruneau [bd], N.K. Pruthi [ah], M. Przybycien [a], P.R. Pujahari [q], J. Putschke [bd], H. Qiu [y], R. Raniwala [am], S. Raniwala [am], R.L. Ray [av], R. Redwine [z], R. Reed [f], C.K. Riley [be], H.G. Ritter [y], J.B. Roberts [an], O.V. Rogachevskiy [u], J.L. Romero [f], J.F. Ross [l], L. Ruan [d], J. Rusnak [n], N.R. Sahoo [ba], P.K. Sahu [p], I. Sakrejda [y], S. Salur [y], A. Sandacz [bb], J. Sandweiss [be], E. Sangaline [f], A. Sarkar [q], J. Schambach [av], R.P. Scharenberg [ak], A.M. Schmah [y], B. Schmidke [d], N. Schmitz [aa], T.R. Schuster [o], J. Seele [z], J. Seger [l], P. Seyboth [aa], N. Shah [g], E. Shahaliev [u], M. Shao [ap], B. Sharma [ah], M. Sharma [bd], S.S. Shi [i], Q.Y. Shou [ar], E.P. Sichtermann [y], R.N. Singaraju [ba], M.J. Skoby [r], D. Smirnov [d], N. Smirnov [be], D. Solanki [am],

0370-2693
http://dx.doi.org/10.1016/j.physletb.2013.01.014

P. Sorensen [d], U.G. deSouza [ao], H.M. Spinka [b], B. Srivastava [ak], T.D.S. Stanislaus [az], S.G. Steadman [z], J.R. Stevens [r], R. Stock [o], M. Strikhanov [ac], B. Stringfellow [ak], A.A.P. Suaide [ao], M.C. Suarez [j], M. Sumbera [n], X.M. Sun [y], Y. Sun [ap], Z. Sun [x], B. Surrow [at], D.N. Svirida [s], T.J.M. Symons [y], A. Szanto de Toledo [ao], J. Takahashi [h], A.H. Tang [d], Z. Tang [ap], L.H. Tarini [bd], T. Tarnowsky [ab], D. Thein [av], J.H. Thomas [y], J. Tian [ar], A.R. Timmins [aw], D. Tlusty [n], M. Tokarev [u], S. Trentalange [g], R.E. Tribble [au], P. Tribedy [ba], B.A. Trzeciak [bb], O.D. Tsai [g], J. Turnau [ag], T. Ullrich [d], D.G. Underwood [b], G. Van Buren [d], G. van Nieuwenhuizen [z], J.A. Vanfossen Jr. [v], R. Varma [q], G.M.S. Vasconcelos [h], F. Videbæk [d], Y.P. Viyogi [ba], S. Vokal [u], S.A. Voloshin [bd], A. Vossen [r], M. Wada [av], F. Wang [ak], G. Wang [g], H. Wang [d], J.S. Wang [x], Q. Wang [ak], X.L. Wang [ap], Y. Wang [ax], G. Webb [w], J.C. Webb [d], G.D. Westfall [ab], C. Whitten Jr. [g], H. Wieman [y], S.W. Wissink [r], R. Witt [ay], W. Witzke [w], Y.F. Wu [i], Z. Xiao [ax], W. Xie [ak], K. Xin [an], H. Xu [x], N. Xu [y], Q.H. Xu [aq], W. Xu [g], Y. Xu [ap], Z. Xu [d], L. Xue [ar], Y. Yang [x], Y. Yang [i], P. Yepes [an], Y. Yi [ak], K. Yip [d,*], I.-K. Yoo [al], M. Zawisza [bb], H. Zbroszczyk [bb], J.B. Zhang [i], S. Zhang [ar], X.P. Zhang [ax], Y. Zhang [ap], Z.P. Zhang [ap], F. Zhao [g], J. Zhao [ar], C. Zhong [ar], X. Zhu [ax], Y.H. Zhu [ar], Y. Zoulkarneeva [u], M. Zyzak [y]

[a] *AGH University of Science and Technology, Cracow, Poland*
[b] *Argonne National Laboratory, Argonne, IL 60439, USA*
[c] *University of Birmingham, Birmingham, United Kingdom*
[d] *Brookhaven National Laboratory, Upton, NY 11973, USA*
[e] *University of California, Berkeley, CA 94720, USA*
[f] *University of California, Davis, CA 95616, USA*
[g] *University of California, Los Angeles, CA 90095, USA*
[h] *Universidade Estadual de Campinas, Sao Paulo, Brazil*
[i] *Central China Normal University (HZNU), Wuhan 430079, China*
[j] *University of Illinois at Chicago, Chicago, IL 60607, USA*
[k] *Cracow University of Technology, Cracow, Poland*
[l] *Creighton University, Omaha, NE 68178, USA*
[m] *Czech Technical University in Prague, FNSPE, Prague, 115 19, Czech Republic*
[n] *Nuclear Physics Institute AS CR, 250 68 Řež/Prague, Czech Republic*
[o] *University of Frankfurt, Frankfurt, Germany*
[p] *Institute of Physics, Bhubaneswar 751005, India*
[q] *Indian Institute of Technology, Mumbai, India*
[r] *Indiana University, Bloomington, IN 47408, USA*
[s] *Alikhanov Institute for Theoretical and Experimental Physics, Moscow, Russia*
[t] *University of Jammu, Jammu 180001, India*
[u] *Joint Institute for Nuclear Research, Dubna, 141 980, Russia*
[v] *Kent State University, Kent, OH 44242, USA*
[w] *University of Kentucky, Lexington, KY 40506-0055, USA*
[x] *Institute of Modern Physics, Lanzhou, China*
[y] *Lawrence Berkeley National Laboratory, Berkeley, CA 94720, USA*
[z] *Massachusetts Institute of Technology, Cambridge, MA 02139-4307, USA*
[aa] *Max-Planck-Institut für Physik, Munich, Germany*
[ab] *Michigan State University, East Lansing, MI 48824, USA*
[ac] *Moscow Engineering Physics Institute, Moscow, Russia*
[ad] *National Institute of Science and Education and Research, Bhubaneswar 751005, India*
[ae] *Ohio State University, Columbus, OH 43210, USA*
[af] *Old Dominion University, Norfolk, VA 23529, USA*
[ag] *Institute of Nuclear Physics PAN, Cracow, Poland*
[ah] *Panjab University, Chandigarh 160014, India*
[ai] *Pennsylvania State University, University Park, PA 16802, USA*
[aj] *Institute of High Energy Physics, Protvino, Russia*
[ak] *Purdue University, West Lafayette, IN 47907, USA*
[al] *Pusan National University, Pusan, Republic of Korea*
[am] *University of Rajasthan, Jaipur 302004, India*
[an] *Rice University, Houston, TX 77251, USA*
[ao] *Universidade de Sao Paulo, Sao Paulo, Brazil*
[ap] *University of Science & Technology of China, Hefei 230026, China*
[aq] *Shandong University, Jinan, Shandong 250100, China*
[ar] *Shanghai Institute of Applied Physics, Shanghai 201800, China*
[as] *SUBATECH, Nantes, France*
[at] *Temple University, Philadelphia, PA 19122, USA*
[au] *Texas A&M University, College Station, TX 77843, USA*
[av] *University of Texas, Austin, TX 78712, USA*
[aw] *University of Houston, Houston, TX 77204, USA*
[ax] *Tsinghua University, Beijing 100084, China*
[ay] *United States Naval Academy, Annapolis, MD 21402, USA*
[az] *Valparaiso University, Valparaiso, IN 46383, USA*
[ba] *Variable Energy Cyclotron Centre, Kolkata 700064, India*
[bb] *Warsaw University of Technology, Warsaw, Poland*
[bc] *University of Washington, Seattle, WA 98195, USA*
[bd] *Wayne State University, Detroit, MI 48201, USA*
[be] *Yale University, New Haven, CT 06520, USA*
[bf] *University of Zagreb, Zagreb, HR-10002, Croatia*

ARTICLE INFO

Article history:
Received 9 June 2012
Received in revised form 29 October 2012
Accepted 7 January 2013
Available online 9 January 2013
Editor: H. Weerts

Keywords:
Polarization
Elastic scattering

ABSTRACT

We report a high precision measurement of the transverse single spin asymmetry A_N at the center of mass energy $\sqrt{s} = 200$ GeV in elastic proton–proton scattering by the STAR experiment at RHIC. The A_N was measured in the four-momentum transfer squared t range $0.003 \leqslant |t| \leqslant 0.035$ $(\text{GeV}/c)^2$, the region of a significant interference between the electromagnetic and hadronic scattering amplitudes. The measured values of A_N and its t-dependence are consistent with a vanishing hadronic spin-flip amplitude, thus providing strong constraints on the ratio of the single spin-flip to the non-flip amplitudes. Since the hadronic amplitude is dominated by the Pomeron amplitude at this $\sqrt{s}$, we conclude that this measurement addresses the question about the presence of a hadronic spin flip due to the Pomeron exchange in polarized proton–proton elastic scattering.

1. Introduction

High energy diffractive hadronic scattering at small values of four-momentum transfer squared t, is dominated by an exchange of the Pomeron trajectory, a color-singlet object with the quantum numbers of the vacuum [1,2]. The calculation of cross-sections for small-t scattering requires a non-perturbative approach in QCD and its theoretical treatment is still being developed. The experimental data therefore provide significant constraints for theoretical approaches and models [3,4]. The coupling of the Pomeron to the nucleon spin is of special interest since it is predicted to be sensitive to the internal dynamics of the nucleon [3,4]. Studies of the spin dependence of proton–proton (pp) scattering at small momentum transfers and at the highest energies presently available at RHIC offer an opportunity to reveal important information on the nature of the Pomeron.

There are several theoretical approaches which predict non-zero spin-dependent Pomeron amplitudes for elastic scattering. Examples include an approach in which the Pomeron–proton coupling is modeled via two-pion exchange [5], an impact picture model assuming that the spin-flip contribution is sensitive to the impact parameter distribution of matter in a polarized proton [6], and a model which treats the Pomeron helicity coupling analogously to that of the isoscalar anomalous magnetic moment of the nucleon [7]. Still another approach assumes a diquark enhanced picture of the proton [8], in which a non-zero spin-flip amplitude may arise if the proton wave function is dominated by an asymmetric configuration, such as a quark–diquark.

Here we present a high precision measurement of the transverse single spin asymmetry A_N in elastic scattering of polarized protons at $\sqrt{s} = 200$ GeV in the t-range $0.003 \leqslant |t| \leqslant 0.035$ $(\text{GeV}/c)^2$ by the STAR experiment [9] at RHIC. The single spin asymmetry A_N is defined as the left–right cross-section asymmetry with respect to the transversely polarized proton beam. In this range of t, A_N originates predominantly from the interference between electromagnetic (Coulomb) spin-flip and hadronic (nuclear) non-flip amplitudes [3]. However, it was realized that A_N in the Coulomb-nuclear interference (CNI) region is also a sensitive probe of the hadronic spin-flip amplitude [8], which will be discussed in more detail in Section 2.

A previous measurement of A_N in a similar t-range and the same $\sqrt{s}$, but with limited statistics, has been reported by the PP2PP Collaboration [10]. Other measurements of A_N performed at small t were obtained at significantly lower energies. They include high precision results from the RHIC polarimeters obtained at $\sqrt{s} = 6.8$–21.7 GeV for elastic proton–proton [11–13] and proton–carbon [14] scattering, as well as earlier results from the BNL AGS for pC scattering [15] at $\sqrt{s} = 6.4$ GeV and from FNAL E704 for pp scattering [16] at $\sqrt{s} = 19.4$ GeV.

The combined analysis of all results, which covers a wide energy range and different targets, will help to disentangle contributions of various exchange mechanisms relevant for elastic scattering in the forward region [17]. In particular, such an analysis will allow us to extract information on the spin dependence of the diffractive mechanism which dominates at high energies.

2. Hadronic spin-flip amplitude in elastic collisions

Elastic scattering of two protons is described by five independent helicity amplitudes: two helicity conserving (ϕ_1 and ϕ_3), two double helicity-flip (ϕ_2 and ϕ_4), and one single helicity-flip amplitude (ϕ_5) — see [3] for definitions. At very high $\sqrt{s}$, such as available at RHIC, and very small $|t| < 0.05$ $(\text{GeV}/c)^2$, the proton mass m can be neglected with respect to $\sqrt{s}$ and t can be neglected with respect to m, which simplifies kinematical factors in the following formulas. The elastic spin-averaged cross-section is given by:

$$\frac{d\sigma}{dt} = \frac{2\pi}{s^2}\left(|\phi_1|^2 + |\phi_2|^2 + |\phi_3|^2 + |\phi_4|^2 + 4|\phi_5|^2\right), \tag{1}$$

while the single spin-flip amplitude ϕ_5 gives rise to the single spin asymmetry, A_N, through interference with the remaining amplitudes:

$$A_N \frac{d\sigma}{dt} = -\frac{4\pi}{s^2}\,\mathrm{Im}\left\{\phi_5^*(\phi_1 + \phi_2 + \phi_3 - \phi_4)\right\}. \tag{2}$$

Each of the amplitudes consists of Coulomb and hadronic contributions: $\phi_i = \phi_i^{\text{em}} + \phi_i^{\text{had}}$, with the electromagnetic one-photon exchange amplitudes ϕ_i^{em} described by QED using the measured anomalous magnetic moment of the proton [18]. The optical theorem relates the hadronic amplitudes to the total cross-section:

$$\sigma_{\text{total}} = \frac{4\pi}{s}\,\mathrm{Im}\left(\phi_1^{\text{had}} + \phi_3^{\text{had}}\right)\Big|_{t=0}, \tag{3}$$

which provides an important constraint on the parameterization of these dominant helicity conserving hadronic amplitudes.

The contribution of the two double spin-flip hadronic amplitudes ϕ_2^{had} and ϕ_4^{had} to the asymmetry A_N is small, as indicated by both experimental results [19,20] and theoretical predictions [21]. Thus, the main contribution to A_N is given by:

$$A_N \frac{d\sigma}{dt} = -\frac{8\pi}{s^2}\,\mathrm{Im}\left(\phi_5^{\text{em}*}\phi_+^{\text{had}} + \phi_5^{\text{had}*}\phi_+^{\text{em}}\right), \tag{4}$$

where $\phi_+ = (\phi_1 + \phi_3)/2$.

* Corresponding author.
E-mail address: kinyip@bnl.gov (K. Yip).

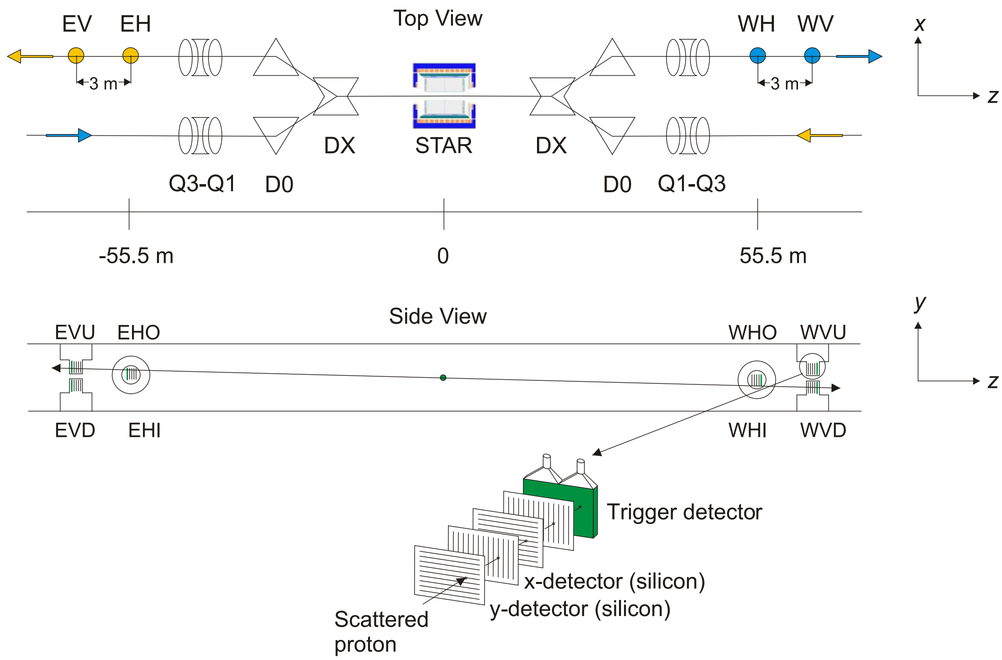

Fig. 1. (Color online.) The layout of the experiment. The Roman Pot stations are located on both sides of the STAR IP. The positive z direction is defined along the outgoing "Blue" beam (the West direction). Positive y is pointing up and positive x is pointing away from the center of the RHIC ring. The detectors are placed on the outgoing beams. The figure is not to scale.

The parametrization of $\phi_5^{\rm had}$ is usually done in terms of $\phi_+^{\rm had}$: $\phi_5^{\rm had}(s,t) = (\sqrt{-t}/m) \cdot r_5(s) \cdot \mathrm{Im}\,\phi_+^{\rm had}(s,t)$, where m is the proton mass. Thus r_5 is the measure of the ratio of the hadronic single spin-flip amplitude (ϕ_5) to hadronic single non-flip amplitudes (ϕ_1 and ϕ_3). Using this parametrization the following representation of A_N can be derived [3]:

$$A_N = \frac{\sqrt{-t}}{m}\frac{[\kappa(1-\rho\delta) + 2(\delta\,\mathrm{Re}\,r_5 - \mathrm{Im}\,r_5)]\frac{t_c}{t} - 2(\mathrm{Re}\,r_5 - \rho\,\mathrm{Im}\,r_5)}{(\frac{t_c}{t})^2 - 2(\rho+\delta)\frac{t_c}{t} + (1+\rho^2)}, \tag{5}$$

where $t_c = -8\pi\alpha/\sigma_{\rm total}$, κ is the anomalous magnetic moment of the proton, $\rho = \mathrm{Re}\,\phi_+/\mathrm{Im}\,\phi_+$ is the ratio of the real to imaginary parts of the non-flip elastic amplitude, and δ is the relative phase between the Coulomb and hadronic amplitudes [3]:

$$\delta = \alpha \ln \frac{2}{|t|(B + 8/\Lambda^2)} - \alpha\gamma, \tag{6}$$

where B is the slope of the forward peak in elastic scattering, $\alpha = 1/137$ is the fine structure constant, $\gamma = 0.5772$ is Euler's constant, and $\Lambda^2 = 0.71\ (\mathrm{GeV}/c)^2$.

3. Detection of elastic proton–proton collisions at RHIC

The protons, which scatter elastically at small angles ($\lesssim$2 mrad), follow the optics of the RHIC magnets and are detected by a system of detectors placed close to the beam inside movable vessels known as "Roman Pots" (RPs) [22]. The Roman Pot stations are located on either side of the STAR interaction point (IP) at 55.5 m and 58.5 m with horizontal and vertical insertions of the detectors, respectively. The coordinate system of the experiment is described in Fig. 1. There are eight Roman Pots, four on each side of the IP. Four approach the beam horizontally WHI, WHO (EHI, EHO) and four approach the beam vertically WVU, WVD (EVU, EVD) as shown in Fig. 1. The location of the RPs was optimized so that, combined with proper accelerator magnet settings, it provides so-called "parallel-to-point focusing", i.e. the (x, y) position of the scattered protons at the RPs depends almost exclusively on their scattering angles and is nearly insensitive to the transverse position of the interaction point. As shown in Fig. 1, there are five major magnets between the RPs and the collision point, two dipole magnets DX and D0, which bend beams into collision, and the focusing triplet of quadrupoles Q1–Q3. The dipole magnets scatter out particles with momentum which is not close to the beam momentum. The detector package inside each RP consists of four 0.4 mm thick silicon micro-strip detector planes with a strip pitch of about 100 μm, two of them measuring the horizontal (x) and two the vertical (y) position of a scattered proton. The sensitive area of the detectors is $79 \times 48\ \mathrm{mm}^2$. Scintillation counters covering this area are used to form a trigger for elastic events. More details on the experiment and the technique can be found in Refs. [22,23].

The preliminary alignment was done by surveying the detector packages during their assembly and after installation inside the Roman Pots with respect to the beam line of the accelerator. The displacement of the RPs during data taking was measured by linear variable differential transformers (LVDTs). The final alignment was done using elastic events in the overlapping regions of horizontal and vertical RPs, which allowed a relative position measurement of the RPs on each side of the IP with a precision better than 0.1 mm. Collinearity of the elastic events and Monte Carlo simulations of the acceptance boundaries due to limiting apertures in the quadrupole magnets were used to further constrain the geometry and to estimate systematic errors.

The data were taken during four dedicated RHIC stores between June 30 and July 4, 2009 with special beam optics of $\beta^* = 22$ m in order to minimize the angular divergence at the IP [24]. The average luminosity over the four stores during which the data were collected was $\mathcal{L} \approx 2 \cdot 10^{29}\ \mathrm{cm}^{-2}\,\mathrm{s}^{-1}$. The closest approach of the first strip to the center of the beam was about 10 mm or about 12σ of the transverse beam size. A total of 33 million elastic triggers were recorded.

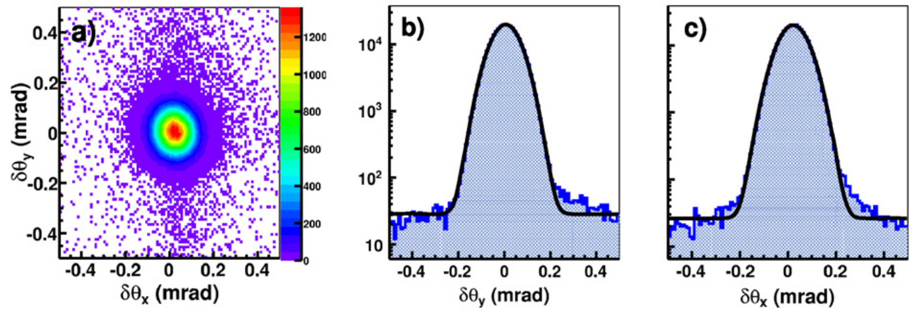

Fig. 2. (Color online.) Distribution of $\delta\theta_y$ vs. $\delta\theta_x$ for both detector pairs in horizontal RPs (a) and their projections in $\delta\theta_y$ (b) and $\delta\theta_x$ (c). The overlaid curves represent the fits with a Gaussian signal and a linear background. The σ values of distributions are ≈58 μrad, consistent with beam angular divergence, and the background-to-signal ratio under the Gaussian distributions in $\pm 3\sigma$ is ≈0.4%.

4. Data selection and reconstruction of elastic scattering events

The selection of elastic events in this experiment is based on the collinearity of the scattered proton tracks. A single track was required on each side of the IP. Noisy and dead strips were rejected, with a total of five out of ≈14 000 in the active detector area. Track reconstruction started with the search for hits in the silicon detectors. First, adjacent strips with collected charge values above 5σ from their pedestal averages were found and combined into clusters. A threshold depending on the cluster width was applied to the total charge of the cluster, thus improving the signal-to-noise ratio for clusters of 3 to 5 strips, while wider clusters were rejected. The cluster position was determined as a charge weighted average of strip coordinates. For each RP a search was performed for matching clusters in the pairs of planes measuring the same coordinate. Two clusters in such planes were considered matched if the distance between them was smaller than 200 μm, approximately the width of two strips. A matching pair with the smallest matching distance was chosen and its cluster coordinates were averaged. If only one cluster in the pair of planes was found, we just use its coordinate for the analysis. If more than one cluster or no match was found, no output from this RP was selected. An (x, y) pair found in an RP was considered a track. About 1/3 of all reconstructed tracks were found in the region of overlapping acceptance between the horizontal and the vertical RPs; for those tracks the average of the kinematic variables was used. To minimize the background contribution from beam halo particles, products of beam–gas interactions, and detector noise, fiducial areas were selected to cut edges of the silicon detectors near the beam and boundaries of the magnet apertures.

Planar angles $\theta_x^{RP}, \theta_y^{RP}$ and coordinates x^{RP}, y^{RP} of protons at a given RP relate to the angles θ_x, θ_y and coordinates x, y at the IP by the transport matrix $\mathbf{M}$:

$$\begin{bmatrix} x^{RP} \\ \theta_x^{RP} \\ y^{RP} \\ \theta_y^{RP} \end{bmatrix} = \mathbf{M} \begin{bmatrix} x \\ \theta_x \\ y \\ \theta_y \end{bmatrix} = \begin{bmatrix} a_{11} & L_x^{\text{eff}} & a_{13} & a_{14} \\ a_{21} & a_{22} & a_{23} & a_{24} \\ a_{31} & a_{32} & a_{33} & L_y^{\text{eff}} \\ a_{41} & a_{42} & a_{43} & a_{44} \end{bmatrix} \begin{bmatrix} x \\ \theta_x \\ y \\ \theta_y \end{bmatrix}. \quad (7)$$

For example, the transport matrix $\mathbf{M}$ for the horizontal Roman Pot in the West side of the IP (WHI,WHO) is:

$$\mathbf{M} = \begin{bmatrix} -0.0913 & 25.2566\ \text{m} & -0.0034 & 0.0765\ \text{m} \\ -0.0396\ \text{m}^{-1} & 0.0137 & -0.0001\ \text{m}^{-1} & 0.0057 \\ -0.0033 & -0.1001\ \text{m} & 0.1044 & 24.7598\ \text{m} \\ 0.0002\ \text{m}^{-1} & 0.0083 & -0.0431\ \text{m}^{-1} & -0.6332 \end{bmatrix}.$$

For the case of parallel-to-point focusing, and in the absence of x–y mixing, the transport matrix is simplified and the so-called "effective" length, L^{eff}, terms dominate. The L^{eff} values are in the range of 22–26 m for this experiment. The angles of the scattered protons at the IP can then be reconstructed independently for the East (E) and West (W) arms with respect to the IP:

$$\theta_x = x^{RP}/L_x^{\text{eff}}, \quad (8)$$

$$\theta_y = y^{RP}/L_y^{\text{eff}}. \quad (9)$$

Because non-dominant terms in the transport matrix are small and result in a negligible correction of about 4 μrad to the reconstruction of the scattering angles, we used a 2×2 matrix (L_x^{eff}, a_{14}; a_{32}, L_y^{eff}), which was obtained by neglecting those small terms of the transport matrix. Once the planar angles at IP were reconstructed, a collinearity requirement was imposed using χ^2 defined as:

$$\chi^2 = \left[(\delta\theta_x - \delta\bar{\theta}_x)/\sigma_{\theta_x}\right]^2 + \left[(\delta\theta_y - \delta\bar{\theta}_y)/\sigma_{\theta_y}\right]^2, \quad (10)$$

where $\delta\theta_{x,y} = [\theta_{x,y}^W - \theta_{x,y}^E]$ and the mean values $\delta\bar{\theta}_{x,y}$ and widths $\sigma_{\theta_{x,y}}$ are taken from the fits to data performed for each data sample. An example is shown in Fig. 2. The small non-zero mean values (≈10 μrad) are consistent with the uncertainties of angle determinations discussed in the next section. Fig. 2 shows a typical distribution of $\delta\theta_y$ vs. $\delta\theta_x$ and its projections, fitted with a Gaussian and a linear background. Based on these fits, the non-collinear background contribution is estimated to be 0.3–0.5%. The requirement of $\chi^2 < 9$ left about 21 million events for the asymmetry calculations.

The polar scattering angle θ and azimuthal angle φ (measured counterclockwise from the positive x axis) for an event were then calculated as an average of those obtained from East and West arms, and the four-momentum transfer squared, t, was assigned to the event using $t = -2p^2(1 - \cos\theta) \approx -p^2\theta^2$ with $p = 100.2$ GeV/c.

5. Single spin asymmetries

The azimuthal angle dependence of the cross-section for the elastic collision of vertically polarized protons is given [25] by:

$$\frac{d^2\sigma}{dt\,d\varphi} = \frac{1}{2\pi}\frac{d\sigma}{dt} \cdot \left[1 + (\mathcal{P}_B + \mathcal{P}_Y)A_N(t)\cos\varphi + \mathcal{P}_B\mathcal{P}_Y\left(A_{NN}(t)\cos^2\varphi + A_{SS}(t)\sin^2\varphi\right)\right], \quad (11)$$

where higher order terms are ignored, $d\sigma/dt$ is the spin-averaged cross-section, $\mathcal{P}_B$ and $\mathcal{P}_Y$ are the beam polarizations for the two colliding beams (called Blue and Yellow). The double spin asymmetry A_{NN} is defined as the cross-section asymmetry for scattering of protons with spin orientations parallel and antiparallel with respect to the unit vector $\hat{n}$, normal to the scattering plane. The asymmetry A_{SS} is defined analogously for both beams fully polarized along the unit vector $\hat{s}$ in the scattering plane and normal to the beam.

Table 1
A_N values in five t ranges with associated uncertainties. Statistical errors for t are negligible and combined systematic errors are shown (see the text for details). Statistical errors and systematic errors on A_N are also shown, where δA_N (syst.) is a scale error due to the beam polarization.

$-t$ [(GeV/c)^2]	0.003–0.005	0.005–0.01	0.01–0.015	0.015–0.02	0.02–0.035
No. of events	444 045	2 091 977	2 854 764	2 882 893	2 502 703
$\langle -t\rangle$ [(GeV/c)^2]	0.0039	0.0077	0.0126	0.0175	0.0232
δt [(GeV/c)^2] (syst.)	0.0001	0.0002	0.0003	0.0004	0.0004
A_N	0.0403	0.0299	0.0227	0.0196	0.0170
δA_N (stat.)	0.0016	0.0008	0.0007	0.0007	0.0007
δA_N (syst.)	0.0021	0.0016	0.0012	0.0010	0.0009

For each of the four RHIC stores, the event sample satisfying the requirements for elastic scattering was divided into five t-bins. Within each t-bin, the φ distributions were subdivided into bins of 10°. The raw asymmetry, $\varepsilon_N(\varphi)$, was calculated using geometric means [26], the so-called "square root formula" for each pair of φ and $\pi-\varphi$ bins in the range $-\pi/2<\varphi<\pi/2$:

$$\begin{aligned}\varepsilon_N(\varphi) &= \frac{(\mathcal{P}_B+\mathcal{P}_Y)A_N\cos(\varphi)}{1+\nu(\varphi)}\\ &= \frac{\sqrt{N^{\uparrow\uparrow}(\varphi)N^{\downarrow\downarrow}(\pi-\varphi)}-\sqrt{N^{\downarrow\downarrow}(\varphi)N^{\uparrow\uparrow}(\pi-\varphi)}}{\sqrt{N^{\uparrow\uparrow}(\varphi)N^{\downarrow\downarrow}(\pi-\varphi)}+\sqrt{N^{\downarrow\downarrow}(\varphi)N^{\uparrow\uparrow}(\pi-\varphi)}},\end{aligned} \quad (12)$$

where the "↑" and "↓" indicate the spin direction of the transversely polarized colliding proton beam bunches, N is the number of events detected in the respective spin and respective φ states and $\nu(\varphi)=\mathcal{P}_B\mathcal{P}_Y(A_{NN}\cos^2(\varphi)+A_{SS}\sin^2(\varphi))$.

In the square root formula (12), the relative luminosities of different spin direction combinations cancel out. In addition, the detector acceptance and efficiency also cancel out, provided they do not depend on the bunch polarization. Results of Ref. [19] and preliminary results of this experiment [20] show that both A_{NN} and A_{SS} are very small ≈ 0.005 (and compatible with zero), constraining $\nu(\varphi)$ to ≈ 0.002, which can be safely neglected.

For each RHIC store, the obtained raw asymmetries were divided by the sum of polarizations of both beams for this particular store, and then averaged over the stores. The resulting asymmetries for each t bin are shown in Fig. 3(a)–(e) as a function of φ. The solid lines represent the best fits to Eq. (12).

Along with the raw asymmetry, ε_N, which is proportional to the sum of the beam polarizations $(\mathcal{P}_B+\mathcal{P}_Y)$, other asymmetries can be obtained using different combinations of bunch spin directions. For instance, the asymmetry proportional to the beam polarization difference $(\mathcal{P}_B-\mathcal{P}_Y)$ is defined as follows:

$$\begin{aligned}\varepsilon'(\varphi) &= \frac{(\mathcal{P}_B-\mathcal{P}_Y)A_N\cos(\varphi)}{1-\nu(\varphi)}\\ &= \frac{\sqrt{N^{\uparrow\downarrow}(\varphi)N^{\downarrow\uparrow}(\pi-\varphi)}-\sqrt{N^{\downarrow\uparrow}(\varphi)N^{\uparrow\downarrow}(\pi-\varphi)}}{\sqrt{N^{\uparrow\downarrow}(\varphi)N^{\downarrow\uparrow}(\pi-\varphi)}+\sqrt{N^{\downarrow\uparrow}(\varphi)N^{\uparrow\downarrow}(\pi-\varphi)}}.\end{aligned} \quad (13)$$

Provided that the beam polarizations ($\mathcal{P}_B$ and $\mathcal{P}_Y$) have the same values, which is approximately valid in this experiment, one would expect $\varepsilon'=0$. The derived values of ε' may be used to estimate false asymmetries, which remain after applying the "square root" method. The distribution of the asymmetry ϵ', obtained for the whole t-range, together with its fit, is shown in Fig. 3(f).

During data taking, 64 bunches (16 ↑↑, 16 ↓↓, 16 ↑↓, 16 ↓↑) of the 90 proton beam bunches collided with usable spin patterns, and were used for ε_N and ε' calculations.

The major systematic uncertainties of the experiment are due to the error of the beam polarization measurement, the reconstruction of t and a small background contribution as shown in Fig. 2. The two main contributions to the uncertainty in the t reconstruction are due to the uncertainties of the L^{eff} values and the position

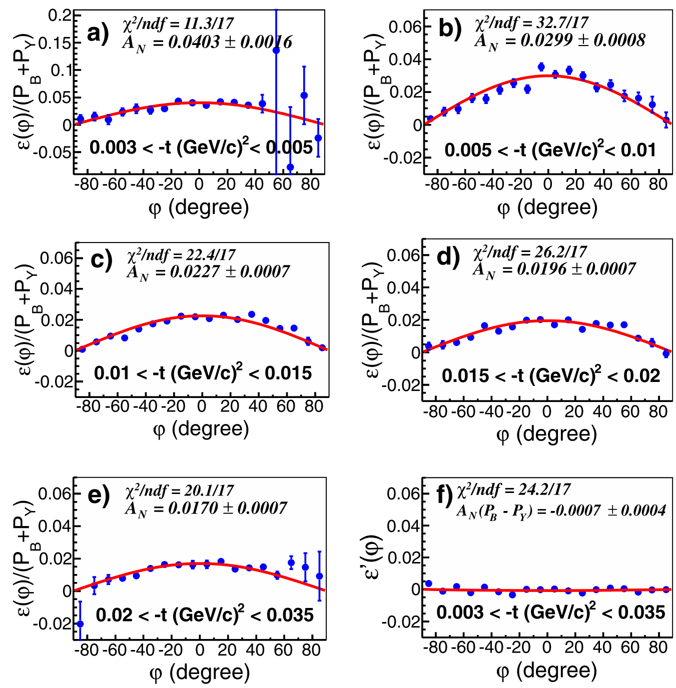

Fig. 3. (Color online.) The asymmetry $\varepsilon(\varphi)/(\mathcal{P}_B+\mathcal{P}_Y)$ for the five t-intervals as given in Table 1 (a)–(e). The asymmetry $\varepsilon'(\varphi)$ for the whole measured t-range (f). The red curves represent the best fit to Eq. (12) (a)–(e) and Eq. (13) (f).

of the beam center at the RP location. The former is mostly due to the uncertainty on values of the magnetic field strength in the Q1–Q3 focusing quadrupoles, which is mainly due to uncertainties in the magnet current and field measurements. The correction to the strength was derived using the correlation between the angle and position in the RPs for the tracks in the regions where the detector acceptance overlaps. An overall correction to the strength of the focusing quadrupoles of 0.5% was applied. The residual systematic error of the field calculation was estimated to be ≈0.5%, leading to ≈1% uncertainty in L^{eff} and ≈1.4% uncertainty in t [27].

The position of the beam center is the reference point for the scattering angle calculations and effectively absorbs a large set of geometrical unknowns such as beam crossing angles and transverse beam positions at the IP, beam shifts from the beam pipe center at the RP location, as well as survey errors. To accommodate all these uncertainties, corrections to the survey were introduced based on the comparison of the simulated to the measured (x, y) distributions at the horizontal RPs on both sides of the IP. The simulation of the transport of elastically scattered protons through the RHIC magnets and the apertures was done and the detector acceptance was calculated. The acceptance boundaries from that simulation and the data were compared. No correction was found for the West side, while for the East side a correction of $(\Delta x, \Delta y) = (2.5, 1.5)$ mm was obtained. The uncertainty of that correction was estimated to be 400 µm. After applying that alignment correction, the collinearity, defined as the average angle difference $\delta\bar{\theta}_{x,y}$ (see Eq. (10)), was reduced from ≈55 µrad to ≈10 µrad. The remaining alignment uncertainty leads to a value of $\delta t/t = 0.0020$ [GeV/c]/$\sqrt{t}$ and was added in quadrature to the uncertainty due to L^{eff}. The number of background events in the data is less than 1% in all t-bins (e.g. see Fig. 2). Assuming the background is beam polarization independent, the asymmetry will be diluted by the same amount, $\delta A_N/A_N < 0.01$. This value results in a negligible contribution to the total error, when statistical and systematic errors are added in quadrature.

The polarization values of the proton beams were determined by the RHIC CNI polarimeter group. Polarizations and their uncertainties (statistical and systematic combined) for the four stores were: 0.623 ± 0.052, 0.548 ± 0.051, 0.620 ± 0.053, 0.619 ± 0.054 (Blue beam), 0.621 ± 0.071, 0.590 ± 0.048, 0.644 ± 0.051, 0.618 ± 0.048 (Yellow beam) [28]. The overall luminosity-weighted average polarization values for all four stores are $\langle \mathcal{P}_B + \mathcal{P}_Y \rangle = 1.224 \pm 0.038$ and $\langle \mathcal{P}_B - \mathcal{P}_Y \rangle = -0.016 \pm 0.038$. Taking into account the overall uncertainty for normalization in polarization measurements, the total polarization error $\delta\langle \mathcal{P}_B + \mathcal{P}_Y \rangle / \langle \mathcal{P}_B + \mathcal{P}_Y \rangle$ is 5.4%.

If the false asymmetry ε_F were proportional to the beam polarization values, it would be indistinguishable from A_N. On the contrary, if it does not depend on the polarization, it contributes equally to both ε_N and ε':

$$\varepsilon_N = A_N(\mathcal{P}_B + \mathcal{P}_Y) + \varepsilon_F, \tag{14}$$

$$\varepsilon' = A_N(\mathcal{P}_B - \mathcal{P}_Y) + \varepsilon_F, \tag{15}$$

and a direct estimate on the false asymmetry can be obtained:

$$\varepsilon_F = \frac{\varepsilon'(\mathcal{P}_B + \mathcal{P}_Y) - \varepsilon_N(\mathcal{P}_B - \mathcal{P}_Y)}{2\mathcal{P}_Y} \approx \varepsilon' - \varepsilon_N \frac{\mathcal{P}_B - \mathcal{P}_Y}{\mathcal{P}_B + \mathcal{P}_Y}. \tag{16}$$

The values of the raw asymmetries, measured in the whole t-range, are $\varepsilon_N = 0.0276 \pm 0.0004$ and $\varepsilon' = -0.0007 \pm 0.0004$. This gives a false asymmetry of $\varepsilon_F = -0.0004 \pm 0.0010$. Thus the conclusion is that the false asymmetry is consistent with zero and very small compared to the measured raw asymmetry ε_N.

The results of the A_N measurements in the five t-bins are summarized in Table 1 together with associated uncertainties and $-t$ range boundaries. Two independent analyses of the data performed with slightly different selection criteria by two different groups gave consistent results. We have also done the cross checks to extract A_N using the beam polarizations of the two beams. The resulting A_N were found to be compatible with those in Table 1 within their statistical uncertainties.

6. Results and conclusions

The measured values of A_N are shown in Table 1 and presented in Fig. 4 together with parameterizations based on formula (5): the dashed line corresponds to no hadronic spin-flip contribution, i.e. $r_5 = 0$, while the solid line is the result of the fit using r_5 as a free parameter. Other parameter values used in the fit are: $\sigma_{\text{total}} = 51.79 \pm 0.12$ mb, $\rho = 0.1278 \pm 0.0015$ taken from fits to the world pp and p$\bar{\text{p}}$ data [29,30] and $B = 16.3 \pm 1.8$ (GeV/c)$^{-2}$ from Ref. [23].

The value of r_5 resulting from the fit described above is shown in Fig. 5 together with 1σ confidence level contours.

In Table 2, we show the central value of the fit and uncertainties on Re r_5 and Im r_5 due to the listed effects. In the first row of the table, the statistical error to the fit with the central value of the parameters is shown. The remaining rows show changes of Re r_5 and Im r_5, when each parameter was varied one by one by $\pm 1\sigma$ during the fit procedure. Rows 2 and 3 show the effect due to the systematic uncertainty in L^{eff} and alignment, row 4 due to the beam polarization (vertical scale uncertainty of A_N) and rows 5–7 systematic contributions due to the uncertainty of fit parameters. The dominant source of the systematic uncertainty

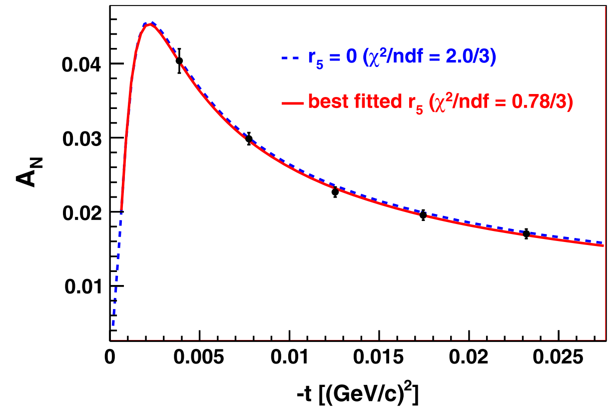

Fig. 4. (Color online.) The measured single spin asymmetry A_N for five $-t$ intervals. Vertical error bars show statistical uncertainties. Statistical error bars in $-t$ are smaller than the plot symbols. The dashed curve corresponds to theoretical calculations without hadronic spin-flip and the solid one represents the r_5 fit.

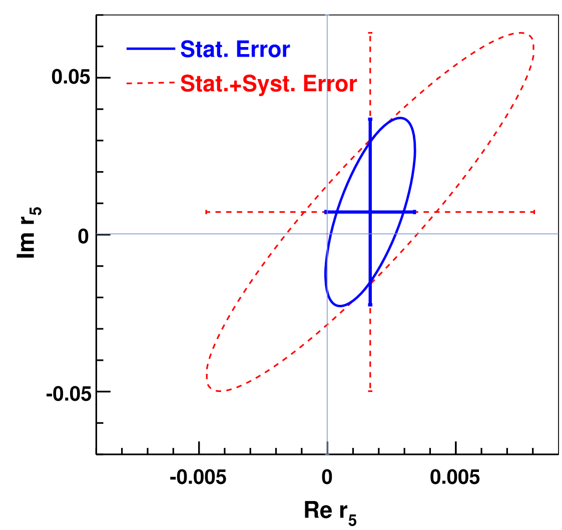

Fig. 5. (Color online.) Fitted value of r_5 with contours corresponding to statistical error only (solid ellipse and cross) and statistical + systematic errors (dashed ellipse and cross) of 1σ.

Table 2
The fitted r_5 values including the uncertainties. (1): Statistical uncertainties. (2)–(4): Systematic uncertainties associated with this measurement. (5)–(7): Systematic uncertainties associated with the values used in the fit function. See the text for details.

	Central value	Re $r_5 = 0.0017$	Im $r_5 = 0.007$
	uncertainties	δ Re r_5	δ Im r_5
1	statistical	0.0017	0.030
2	δt (L^{eff})	0.0008	0.005
3	δt (alignment)	0.0011	0.011
4	$\delta\mathcal{P}$	0.0059	0.047
5	$\delta\sigma_{\text{total}}$	0.0003	0.002
6	$\delta\rho$	<0.0001	<0.001
7	δB	<0.0001	<0.001
	total syst. error	0.0061	0.049
	total stat. + syst. error	0.0063	0.057

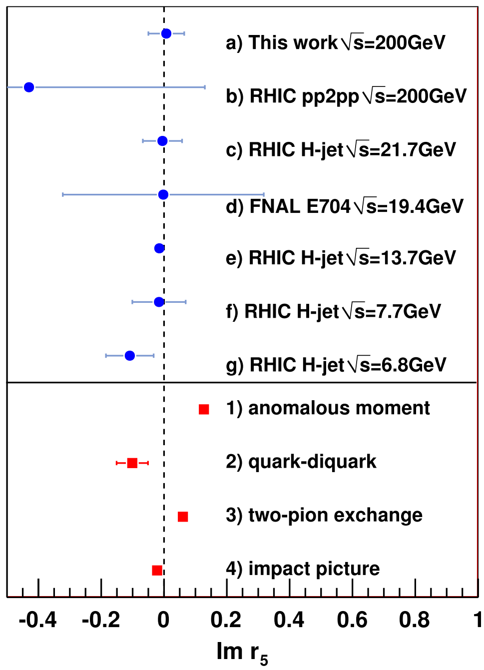

Fig. 6. (Color online.) Measurements of $\mathrm{Im}(r_5)$ values for (a) this experiment, (b) RHIC pp2pp at $\sqrt{s} = 200$ GeV [10], (c) RHIC H-jet target at $\sqrt{s} = 21.7$ GeV [13], (d) FNAL E704 at $\sqrt{s} = 19.4$ GeV [16], (e) RHIC H-jet target at $\sqrt{s} = 13.7$ GeV [11], (f) RHIC H-jet target at $\sqrt{s} = 7.7$ GeV [13], and (g) RHIC H-jet target at $\sqrt{s} = 6.8$ GeV [12]. Theoretical calculations shown are (1) anomalous moment [7], (2) quark–diquark picture [8], (3) two-pion exchange model [5], and (4) impact picture [6]. The theoretical calculations are either energy independent (1, 2, 3) or done at $\sqrt{s} = 200$ GeV (4). The vertical dashed line indicates where $\mathrm{Im}(r_5) = 0$. All error bars shown include both statistical and systematic errors.

is due to the beam polarization uncertainty. The total systematic uncertainty, including the effects related to rows 2–7 of Table 2, is obtained by adding the error covariance matrices. The final result on r_5 is shown in Fig. 5 together with both statistical and systematic uncertainties. The obtained values $\mathrm{Re}\, r_5 = 0.0017 \pm 0.0063$ and $\mathrm{Im}\, r_5 = 0.007 \pm 0.057$ are consistent with the hypothesis of no hadronic spin-flip contribution at the energy of this experiment.

Since the maximum A_N in the CNI region can be evaluated as $\kappa - 2\,\mathrm{Im}\, r_5$ in Eq. (5), theoretical calculations emphasize values of $\mathrm{Im}\, r_5$. Measurements of $\mathrm{Im}\, r_5$ at different energies in the range 6.8 GeV $\leqslant \sqrt{s} \leqslant$ 200 GeV are shown in Fig. 6, together with predictions of theoretical models of the hadronic spin-flip amplitude as discussed above. All of the experimental results, including that reported here, are consistent with the assumption of no hadronic spin-flip contribution to the elastic proton–proton scattering. The high accuracy of the current measurement provides strong limits on the size of any hadronic spin-flip amplitude at this high energy, hence significantly constraining theoretical models which require hadronic spin-flip.

Acknowledgements

We thank the RHIC Operations Group and RCF at BNL, the NERSC Center at LBNL and the Open Science Grid consortium for providing resources and support. This work was supported in part by the Offices of NP and HEP within the US DOE Office of Science, the US NSF, the Sloan Foundation, CNRS/IN2P3, FAPESP CNPq of Brazil, Ministry of Ed. and Sci. of the Russian Federation, NNSFC, CAS, MoST, and MoE of China, GA and MSMT of the Czech Republic, FOM and NWO of the Netherlands, DAE, DST, and CSIR of India, Polish Ministry of Sci. and Higher Ed., National Research Foundation (NRF-2012004024), Ministry of Sci., Ed. and Sports of the Rep. of Croatia, and RosAtom of Russia.

References

[1] V. Barone, E. Predazzi, High-Energy Particle Diffraction, Texts and Monographs in Physics, Springer-Verlag, ISBN 3540421076, 2002.
[2] S. Donnachie, G. Dosch, P. Landshoff, Pomeron Physics and QCD, Cambridge University Press, ISBN 9780521675703, 1998.
[3] N.H. Buttimore, et al., Phys. Rev. D 59 (1999) 114010.
[4] T.L. Trueman, Phys. Rev. D 77 (2008) 054005.
[5] J. Pumplin, G. Kane, Phys. Rev. D 11 (1975) 1183.
[6] C. Bourrely, J. Soffer, T.T. Wu, Phys. Rev. D 19 (1979) 3249; C. Bourrely, J. Soffer, T.T. Wu, Nucl. Phys. B 247 (1984) 15.
[7] M.G. Ryskin, Yad. Fiz. 46 (1987) 611, Sov. J. Nucl. Phys. 46 (1987) 337.
[8] B.Z. Kopeliovich, B.G. Zakharov, Phys. Lett. B 226 (1989) 156.
[9] K.H. Ackermann, et al., Nucl. Instrum. Methods A 499 (2003) 624.
[10] S. Bültmann, et al., Phys. Lett. B 632 (2006) 167.
[11] H. Okada, et al., Phys. Lett. B 638 (2006) 450.
[12] I.G. Alekseev, et al., Phys. Rev. D 79 (2009) 094014.
[13] A. Bazilevsky, et al., in: Proceedings of SPIN 2010, J. Phys. Conf. Ser. 295 (2011) 012096.
[14] O. Jinnouchi, et al., in: F. Bradamante, et al. (Eds.), Proceedings of the 16th International Spin Physics Symposium SPIN 2004, World Scientific, 2005.
[15] J. Tojo, et al., Phys. Rev. Lett. 89 (2002) 052302.
[16] N. Akchurin, et al., Phys. Rev. D 48 (1993) 3026.
[17] T.L. Trueman, in: F. Bradamante, et al. (Eds.), Proceedings of the 16th International Spin Physics Symposium SPIN 2004, World Scientific, 2005.
[18] N.H. Buttimore, et al., Phys. Rev. D 18 (1978) 694.
[19] S. Bültmann, et al., Phys. Lett. B 647 (2007) 98.
[20] I.G. Alekseev, for the STAR Collaboration, J. Phys. Conf. Ser. 295 (2011) 012098.
[21] T.L. Trueman, arXiv:hep-ph/0604153.
[22] S. Bültmann, et al., Nucl. Instrum. Methods A 535 (2004) 415.
[23] S. Bültmann, et al., Phys. Lett. B 579 (2004) 245.
[24] A. Drees, BNL Collider-Accelerator Department Note C-A/AP/441, 2012.
[25] E. Leader, Spin in Particle Physics, Cambridge University Press, 2001.
[26] G.G. Ohlsen, P.W. Keaton Jr., Nucl. Instrum. Methods 109 (1973) 41.
[27] P. Pile, et al., in: Proceedings of 2012 International Particle Accelerator Conference (IPAC12), 2012, p. 1131..
[28] CNI Polarimeter Group at BNL, http://www.rhic.bnl.gov/~cnipol/pubdocs/Run09Offline.
[29] COMPETE Collaboration, http://nuclth02.phys.ulg.ac.be/compete/predictor/.
[30] C. Bourrely, et al., Phys. Rev. D 76 (2007) 053002.